REFERECT 08.05.2006.

Analysis and Design of Marine Structures subjected to Accidental Loads

Response of structures exposed to explosion

$$F \cdot W = \int_0^{\infty} P(x) \cdot dx$$

TO THINK TO MEGASBACK.

masse skulet i last impuls

2 lengde bredde

Splitt interaksjon plate.

June 20, 2005
Jørgen Amdahl, NTNU,
Dept. Marine Technology

Content

1. Mechanism models for plates subjected to uniform lateral load 3
1.1 Rectangular plate undergoing finite deflection 5
2. Mechanism models for beams subjected uniform lateral load 14
2.1 Beams with partial end fixity 17
3. Dynamic behaviour models 19
3.1 Analytic solutions 26
3.2 Approximate solutions for elastic- and plastic periods of vibration 29
3.3 Strain rate effects 31
3.4 Comparison with experimental data 32

1. Mechanism models for plates subjected to uniform lateral load

A collapse model for a rectangular plate subjected to uniform lateral load is shown in Figure 1.1. The boundaries are fixed against rotations but free to slide inwards so that no membrane force is developed.

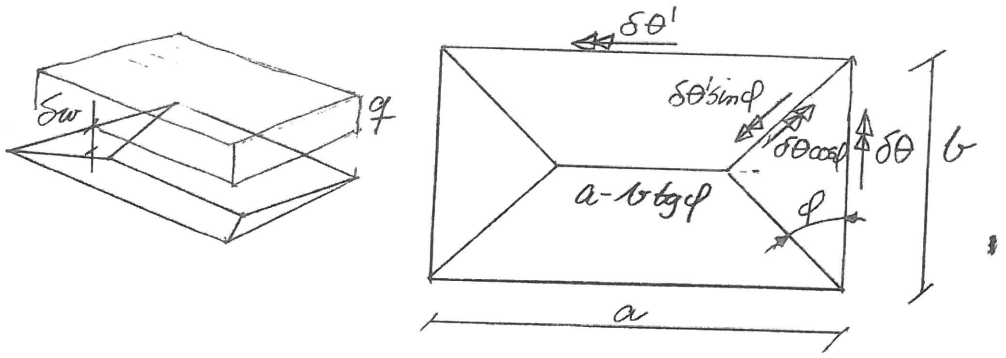

Figure 1.1 Collapse model for rectangular plate

The "roof-top" mechanism assumed is such that plate segments bounded by yield lines rotate as rigid bodies. All energy dissipation takes place in yield lines. The angle of θ of the oblique yield lines is unknown. The virtual rotations along the boundaries are given by

$$\delta\theta = \frac{\delta w}{\frac{b}{2} tg\phi} \tag{1.1}$$

$$\delta\theta^1 = \frac{\delta w}{\frac{b}{2}} = tg\phi\delta\theta \tag{1.2}$$

where δw is the virtual displacement at center.

The internal virtual work is given by

$$\begin{aligned}\delta W_i &= M_P\left\{2atg\phi\delta\theta + 2b\delta\theta + (a-btg\phi)2tg\phi\delta\theta + \frac{2b}{\cos\phi}(\cos\phi\delta\theta + \sin\phi tg\phi\delta\theta)\right\} \\ &= 4MP\{atg\phi + b\}\delta\theta\end{aligned} \tag{1.3}$$

The external virtual work corresponds to the volume of the roof top

$$\begin{aligned}\delta w_e &= \int_A q\delta w(x,y) \\ &= q\left\{(a-btg\phi)btg\phi\, b\frac{\delta w}{3}\right\} \\ &= \frac{q}{12}\{3ab - b^2tg\phi\}btg\phi\delta\theta\end{aligned} \tag{1.4}$$

Equating internal virtual work and external virtual work there comes out

$$q = \frac{48M_P}{b^2}\frac{tg\theta + \frac{b}{a}}{3tg\phi - \frac{b}{a}tg^2\phi} \tag{1.5}$$

The angle ϕ is determined such that q attains a minimum, i.e.:

$$\frac{dq}{d\phi} = 0 \tag{1.6}$$

which yields

$$tg\phi = \sqrt{3 + \left(\frac{b}{a}\right)^2} - \frac{b}{a} \tag{1.7}$$

The corresponding collapse load is

$$q = \frac{48M_P}{b^2}\left(\frac{1}{\sqrt{3 + \left(\frac{b}{a}\right)^2} - \frac{b}{a}}\right)^2 \tag{1.8}$$

In case of simply supported edges the internal virtual work is halved and the collapse load becomes

$$q = \frac{24M_P}{b^2}\left(\frac{1}{\sqrt{3+\left(\frac{b}{a}\right)^2}-\frac{b}{a}}\right)^2 \tag{1.9}$$

1.1 Rectangular plate undergoing finite deflection

When the deflections at the centre of the plate become finite, membrane forces develop which increase the load-carrying capacity. As a first step consider the deformation of a plate strip with unit width in Figure 1.2

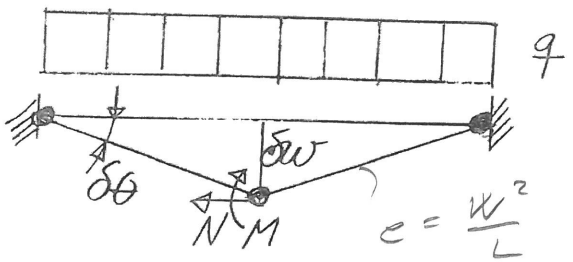

Figure 1.2 Collapse mechanism for plate strip

The internal virtual work in one hinge is

$$\delta W_i = M\delta\theta + N\delta u \tag{1.10}$$

The virtual elongation in a hinge is found from kinematic considerations

$$\delta u = \frac{w}{2}\delta\theta \tag{1.11}$$

The bending moment and axial force must further satisfy the plastic interaction function for a platestrip, being

$$\Gamma = \frac{M}{M_P} + \left(\frac{N}{N_P}\right)^2 - 1 = 0 \tag{1.12}$$

where

$N_p = \sigma_y h$ is plastic axial capacity

$M_p = \sigma_y \frac{h^2}{4}$ is plastic bending moment for platestrip of thickness h

The normality criterion states that

$$\delta u = \delta\lambda \frac{\partial \Gamma}{\partial N} = \delta\lambda \frac{2N}{N_p^2} \tag{1.13}$$

$$\delta\theta = \delta\lambda \frac{\partial \Gamma}{\partial M} = \delta\lambda \frac{1}{M_p} \tag{1.14}$$

Combining Equations **(1.11)** , **(1.13)**, **(1.14)** there comes out

$$\frac{N}{N_p} = \frac{w}{h} \tag{1.15}$$

The internal virtual work is now

$$\begin{aligned} \delta W_i &= M_P \left\{ 1 - \left(\frac{N}{N_P} \right)^2 + \frac{N_P}{M_P} \frac{N}{N_P} \frac{w}{2} \right\} \delta\theta \\ &= M_P \left\{ \left(1 - \left(\frac{w}{h} \right)^2 + 2 \left(\frac{w}{h} \right)^2 \right) \right\} \delta\theta \end{aligned} \tag{1.16}$$

The first term in Equation **(1.16)** is due to bending and the second is the contribution from membrane forces.

Returning to the rectangular plate, the displacement field introduced pre-supposes that all elongation takes place at the mid hinge, and no elongation at the boundaries. Assigning all virtual work due to membrane forces to the internal hinges we get

$$\delta W_i = M_P \left\{ 1 + 3 \left(\frac{w}{h} \right)^2 \right\} \delta\theta \tag{1.17}$$

For the hinges at the boundaries the following virtual work expression applies

$$\delta W_i = M_P \left\{ 1 - \left(\frac{w}{h} \right)^2 \right\} \delta\theta \tag{1.18}$$

The total internal work is found by integration of Equations **(1.17)** and **(1.18)** along the yield lines. It is further pre-supposed that the angle ϕ of the oblique yield lines is determined during the pure bending phase. Thus, the first term in Equations **(1.17)** and **(1.18)** will remain as in the calculations in Section 5.1.

The integration must now be split up into several regions, see Figure 1.3. The total internal virtual work is four times the hinges indicated.

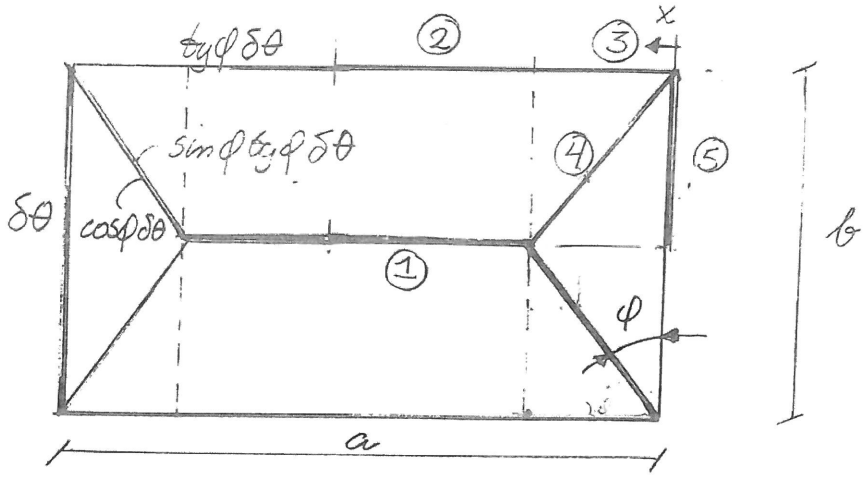

Figure 1.3 Different regions of integration

For the purpose of simply the second term in Equations **(1.17)** and **(1.18)** are shown here

Mid hinges:

$$\frac{\delta W_i^{(1)}}{M_P} = 3\left(\frac{w}{h} \right)^2 (a - b\,tg\phi)\, tg\phi\delta\theta \cdot 2 \tag{1.19}$$

Boundaries in region (2)

$$\frac{\delta W_i^{(2)}}{M_P} = -\left(\frac{w}{h} \right)^2 (a - b\,tg\phi)\, tg\phi\delta\theta \cdot 2 \tag{1.20}$$

Boundaries in region (3):

Here the virtual work expression varies due to the linear variation of w along the oblique yield line. The deflection at coordinate x is given by

$$\frac{w(x)}{h} = \frac{w}{h}\frac{x}{\frac{b}{2}tg\phi} \tag{1.21}$$

This yields

$$\begin{aligned}\frac{\delta W_i^{(3)}}{M_P} &= \int_0^{\frac{b}{2}tg\phi} -\left(\frac{w}{h}\right)^2\left(\frac{x}{\frac{b}{2}tg\phi}\right)^2 dx\cdot tg\phi\delta\theta\cdot 4 \\ &= -\frac{1}{3}\left(\frac{w}{h}\right)^2 2btg^2\phi\delta\theta\end{aligned} \tag{1.22}$$

In oblique yield lines there is obtained similarity

$$\frac{\delta W_i^{(4)}}{M_p} = \left(\frac{w}{h}\right)^2\cdot\frac{b}{2\cos\phi}\{\cos\phi+\sin\phi tg\phi\}\delta\theta\cdot 4 \tag{1.23}$$

At short edge

$$\frac{\delta W_i^{(5)}}{M_p} = \frac{1}{3}\left(\frac{w}{h}\right)^2\cdot b\delta\theta\cdot 2 \tag{1.24}$$

The total virtual work becomes (second term only)

$$\frac{\delta W_i}{M_p}\left(\frac{w}{h}\right)^2\left\{4atg\phi-\frac{8}{3}btg^2\phi+\frac{4}{3}b\right\} \tag{1.25}$$

The total collapse pressure is now given by (confer also Equations **(1.8)** and **(1.9)**)

$$q = \frac{48M_p}{b^2}\frac{tg\phi+\frac{b}{a}}{3tg\phi-\frac{b}{a}tg^2\theta}\left\{1+\left(\frac{w}{h}\right)^2\frac{1}{3}\frac{3tg\phi-2\frac{b}{a}tg^2\phi+\frac{b}{a}}{tg\phi+\frac{b}{a}}\right\} \tag{1.26}$$

The expression for the minimum angle is now introduced (Equation 5.8) in a slightly modified form by defining the parameter

$$\alpha = \frac{b}{a}\left\{\sqrt{3+\left(\frac{b}{a}\right)^2} - \frac{b}{a}\right\} \tag{1.27}$$

which also implies

$$tg\phi = \sqrt{3-2\alpha} \quad \textbf{or} \quad \frac{a}{b} = \frac{\sqrt{3-2\alpha}}{\alpha} \tag{1.28}$$

Equation **(1.26)** can then be written as:

$$q = \frac{48M_p}{a^2\alpha^2}\left\{1+\frac{\alpha+(3-2\alpha)^2}{9-3\alpha}\right\} \tag{1.29}$$

This equation is valid until $w/h = 1$. After this, the axial force becomes equal to the plastic membrane force at the mid hinge. In the oblique hinge lines we have to divide into two parts, one where the axial force is equal to the plastic axial force and one part in which bending moment remains.

The internal virtual work for a platestrip yielding in tension is

$$\delta W_i = N_P \delta u = 4M_P \frac{w}{h}\delta\theta \tag{1.30}$$

and replaces the expression given by Equation **(1.17)**. At the same time the virtual work at the corresponding boundary hinge vanishes. The internal virtual work consists now of the following contributions:

Mid hinges:

$$\frac{\delta W^{(1)}}{M_P} = 4\frac{w}{h}\{a - btg\phi\}\, tg\phi\delta\theta \cdot 2 \tag{1.31}$$

Boundaries in region (2)

$$\frac{\delta W^{(2)}}{M_P} = 0 \tag{1.32}$$

Boundaries in region (3)

$$\frac{\delta W^{(3)}}{M_P} = \int_0^{\frac{\frac{b}{2}tg\phi}{w/h}} \left\{1-\left(\frac{w}{h}\right)^2\left(\frac{x}{\frac{b}{2}tg\phi}\right)^2\right\} dx tg\phi\delta\theta\cdot 4 = \frac{4}{3}\frac{btg^2\phi}{w/h} \tag{1.33}$$

for $x > \dfrac{\frac{b}{2}tg\phi}{w/h}$ the virtual work vanishes in this region.

Oblique yield lines:

$$\begin{aligned}\frac{\delta W^{(4)}}{M_P} &= \int_0^{\frac{b/2\cos\phi}{w/h}} (1+3\left(\frac{w}{h}\right)^2\left(\frac{x}{b/\cos\phi}\right) dx\{\cos\phi+\sin\phi tg\phi\}\,\delta\theta\cdot 4 \\ &+ \int_{\frac{b/2\cos\phi}{w/h}}^{b/2\cos\phi} 4\frac{w}{h}\left(\frac{x}{b/2\cos\phi}\right) dx\{\cos\phi+\sin\phi tg\phi\}\delta\theta\cdot 4\end{aligned} \tag{1.34}$$

$$\begin{aligned}\frac{\delta W^{(4)}}{M_P} &= \frac{4b}{w/h}\{1+tg^2\phi\}\,\delta\theta + 4b\{1+tg^2\phi\}\left\{\frac{w}{h}-\frac{1}{w/h}\right\}\delta\theta \\ &= 4b\{1+tg^2\phi\}\frac{w}{h}\end{aligned} \tag{1.35}$$

Boundaries short edge:

$$\begin{aligned}\frac{\delta W^{(5)}}{M_P} &= \int_0^{\frac{b/2}{w/h}} \left\{1-\left(\frac{w}{h}\right)^2\left(\frac{x}{b/2}\right)^2\right\} dx\delta\theta\cdot 4 \\ &= \frac{4}{3}\frac{b}{w/h}-\delta\theta\end{aligned} \tag{1.36}$$

For $x > \dfrac{b/2}{w/h}$ the virtual work vanishes.

The total virtual work is then

$$\frac{\delta W_i}{M_P} = \frac{w}{h}\left\{8atg\phi - 8btg^2\phi + 4b + 4btg^2\phi\right\}\delta\theta + \frac{1}{3w/h}\left\{4btg\phi + 4b\right\}$$
$$= \frac{w}{h}\left\{8atg\phi + 8b\right\}\left\{1 + \frac{4btg^2\phi + 4b}{8atg\phi + 8b}\left(\frac{1}{3w/h} - 1\right)\right\} \tag{1.37}$$

Introducing $tg\phi = \sqrt{3-2\alpha}$ and $\frac{a}{b} = \frac{\sqrt{3-2\alpha}}{\alpha}$ the following relation holds true:

$$\frac{4btg^2\phi + 4b}{8atg\phi + 8b} = \frac{\alpha(2-\alpha)}{3-\alpha} \tag{1.38}$$

The first term in Equation (5.39) is twice the internal work in pure bending.

Hence,

$$q = \frac{96M_P}{a^2}\frac{w}{h}\left\{1 + \frac{\alpha(2-\alpha)}{3-\alpha}\left(\frac{1}{3(w/h)^2} - 1\right)\right\} \tag{1.39}$$

Similar calculations may be carried out of a simply supported plate. The derived relationship can be summarized by the following formulas:

$$\frac{q}{q_0} = 1 + z^2 \frac{\alpha + (3-2\alpha)^2}{9-3\alpha} \quad , \quad z \le 1 \tag{1.40}$$

$$\frac{q}{q_0} = 2z\left\{1 + \frac{\alpha(2-\alpha)}{3-\alpha}\left(\frac{1}{3z^2} - 1\right)\right\}, \quad z \ge 1 \tag{1.41}$$

where for clamped plate

$$z = \frac{w}{h}, \qquad q_0 = \frac{48 M_P}{a^2 \alpha^2} \tag{1.42}$$

for simply supported plate

$$z = \frac{2w}{h}, \; q_0 = \frac{24 M_P}{a^2 \alpha^2} \tag{1.43}$$

and

$$\alpha = \frac{b}{a}\left\{\sqrt{3 + \left(\frac{b}{a}\right)^2} - \frac{b}{a}\right\} \tag{1.44}$$

$$M_P = \sigma_y \frac{h^2}{4} \tag{1.45}$$

Note the similarity between Equations **(1.40)** and **(1.41)** and those derived for a plate strip previously. In fact, by letting $b/a \to 0$, Equations **(1.40)** and **(1.41)** condensate to the platestrip relationships, namely

$$\frac{q}{q_0} = 1 + z^2 \tag{1.46}$$

$$\frac{q}{q_0} = 2z \tag{1.47}$$

Equations **(1.40)** and **(1.41)** are plotted in Figure 1.4 for different aspects ratios.

Approximate formulas which are valid over the entire deformation range may be obtained by an elliptic fit to the asymptotic solutions

$$\frac{q}{q_0} = 1 \qquad z \to 0 \tag{1.48}$$

$$\begin{aligned} \frac{q}{q_0} &= 2z\left\{1 - \frac{\alpha(2-\alpha)}{3-\alpha}\right\} \\ &= 2z\left\{\frac{1+(\alpha-1)(\alpha-2}{3-\alpha}\right\} \qquad z \to \infty \\ &= 2zf(\alpha) \end{aligned} \tag{1.49}$$

Thus from the equation

$$\left(\frac{1}{q/q_0}\right)^2 + \left\{\frac{2zf(\alpha)}{(q/q_0}\right\}^2 = 1 \tag{1.50}$$

there is obtained

$$\frac{q}{q_0} = \sqrt{1 + \left\{2z\frac{(1+(\alpha-1)(\alpha-2)}{3-\alpha}\right\}} \tag{1.51}$$

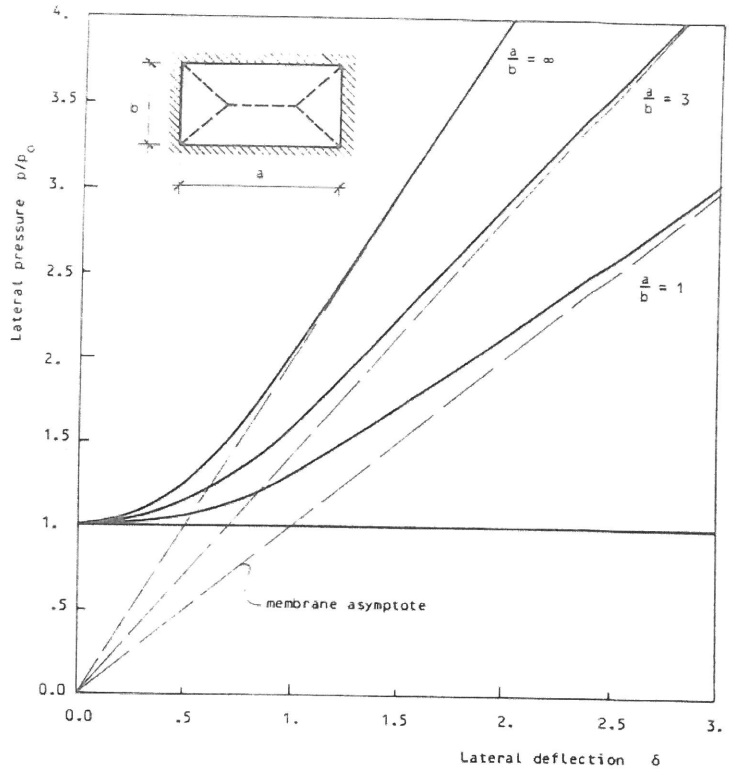

Figure 1.4 Plastic load carrying capacity of rectangular plates with finite deflections

2. Mechanism models for beams subjected uniform lateral load

Equations **(1.46)** and **(1.47)** predict the large displacement behaviour of a beam with a rectangular cross-sections, i.e., cross-sections obeying the plastic interaction curve

$$F = \frac{M}{M_P} + \left(\frac{N}{N_P}\right)^2 - 1 = 0 \qquad (2.1)$$

As shown in Figure 2.1 this expression is too optimistic for I-profiles. A fairly good approximation can be obtained with the interaction curve

$$F = \frac{M}{M_P} + \left(\frac{N}{N_P}\right)^{\alpha} - 1 = 0 \qquad (2.2)$$

where

$1 < \alpha < 2$

This expression can be used to derive plastic-load displacement similar to the ones for rectangular section.

For a fully clamped beam equilibrium is given by (see Figure 2.2)

$$\frac{1}{2}ql = 8\frac{M}{l} + 4N\frac{w}{l} \qquad (2.3)$$

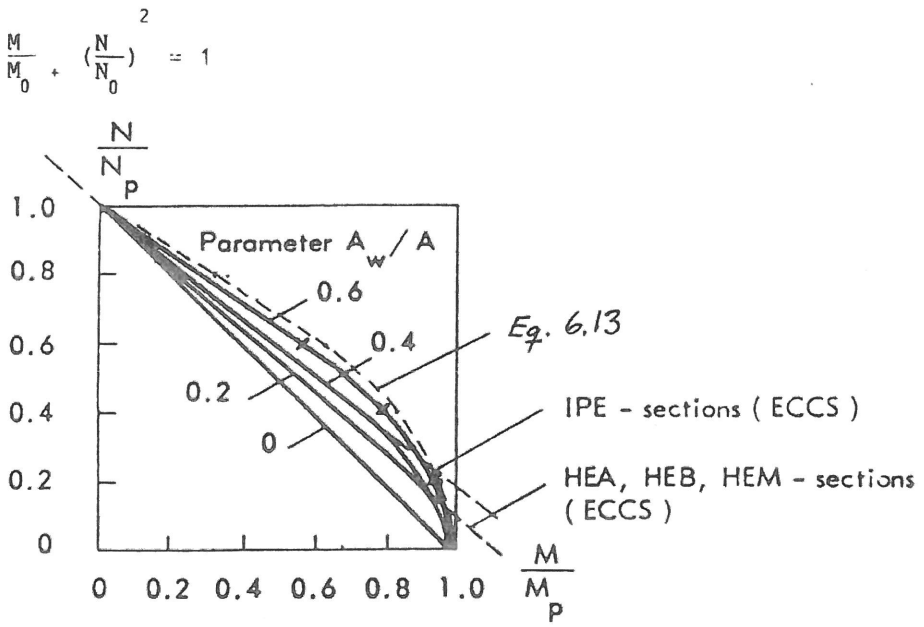

Figure 2.1 Interaction curves for I-profiles

Kinematics yield the following relationship

$$\delta u = \frac{w}{2}\delta\theta \qquad (2.4)$$

The normality criterion requires

$$\delta u = \delta\lambda\alpha \frac{1}{N_P}\left(\frac{N}{N_P}\right)^{\alpha-1} \tag{2.5}$$

$$\delta\theta = \delta\lambda \frac{1}{M_P} \tag{2.6}$$

so that

$$\left(\frac{N}{N_P}\right) = \left(\frac{1}{\alpha}\frac{w}{2}\frac{N_P}{M_P}\right)^{\frac{1}{\alpha-1}} \tag{2.7}$$

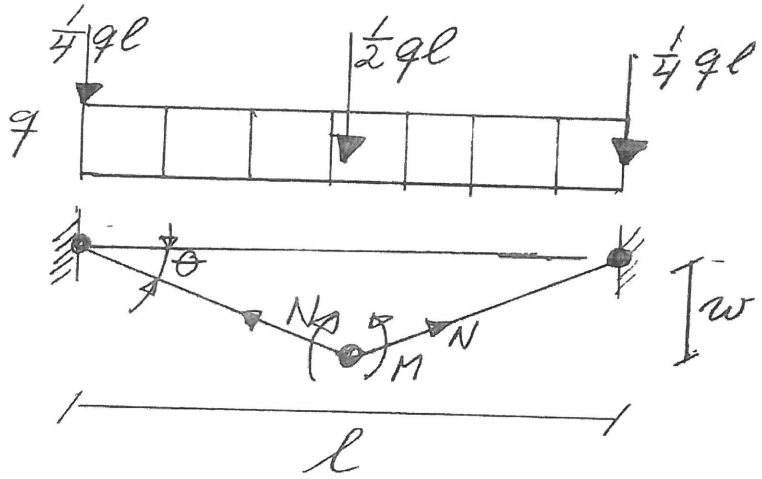

Figure 2.2 Collapse mechanism for beam

Introduction Equations **(2.2)** and **(2.7)** into Equation **(2.3)** there is obtained

$$\frac{q}{q_0} = 1 + \left(\frac{w}{2\alpha}\frac{N_P}{M_P}\right)^{\frac{\alpha}{\alpha-1}}(\alpha-1), \qquad \frac{w}{2\alpha}\frac{N_P}{M_P} \le 1 \tag{2.8}$$

For $\frac{w}{2\alpha}\frac{N_P}{M_P} \ge 1$ the beams becomes a membrane whereby

$$\frac{q}{q_0} = \frac{w}{2}\frac{N_P}{M_P} \tag{2.9}$$

$q_0 = \dfrac{16M_P}{\ell^2}$ denotes the plastic collapse loan in bending

Similar calculations may be performed for a beam with simply supported ends. The results may be summarized as shown in expression **(2.10)**and**(2.11)**.

$$\frac{q}{q_0} = 1 + \delta^{\frac{\alpha}{\alpha-1}}(\alpha - 1) \qquad \delta < 1 \tag{2.10}$$

$$\frac{q}{q_0} = \alpha\delta \qquad \delta > 1 \tag{2.11}$$

where for clamped beam

$$\delta = \frac{w}{2\alpha}\frac{N_P}{M_P} \qquad q_0 = 16\frac{M_P}{\ell^2} \tag{2.12}$$

and simply supported beam

$$\delta = \frac{w}{\alpha}\frac{N_P}{M_P} \qquad q_0 = 8\frac{M_P}{\ell^2} \tag{2.13}$$

2.1 Beams with partial end fixity

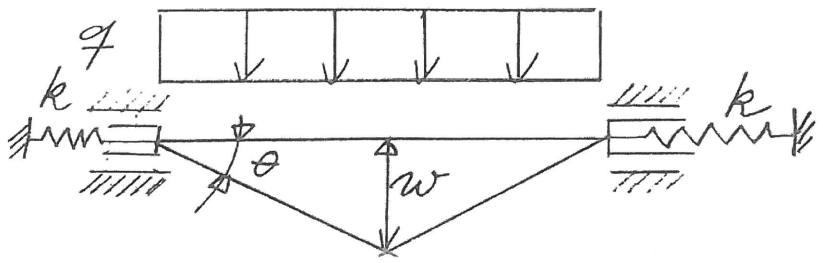

Figure 2.3 Collapse mechanism for beam with partial end fixity

If the beam has a finite axial restraint, the ends will move inwards and thereby relax the build-up of membrane forces. As shown for a tubular beam in Figure 2.3, the virtual plastic elongation in each is now given by

$$\delta u = \frac{w}{2}\delta\theta - \frac{1}{2k}\frac{\partial N}{\partial}\delta\theta \tag{2.14}$$

The normally criterion yields

$$\alpha\frac{1}{N_P}\left(\frac{N}{N_P}\right)^{\alpha-1} = \left\{\frac{w}{2} - \frac{1}{2k}\frac{\partial N}{\partial\theta}\right\}\frac{1}{M_P} \tag{2.15}$$

which also can be expressed as

$$\left(\frac{N}{N_P}\right)^{\alpha-1} = \frac{wN_P}{2\alpha M_P} - \frac{N_P^3\ell}{8k\alpha^2 M_P^2}\frac{\partial\frac{N}{N_P}}{\partial\frac{w}{2\alpha}\frac{N_P}{M_P}} \tag{2.16}$$

A simpler notation is

$$n^{\alpha-1} = \delta - \frac{1}{c}\frac{dn}{d\delta} \tag{2.17}$$

where the dimensionless spring constant is defined by

$$c = \frac{N_P^3\ell}{8k\alpha^2 M_P^2} \tag{2.18}$$

FC DETTE ER TV. SVITT KONSTANT.

A closed-form solution of Equation **(2.18)** is difficult. Instead numerical integration is used, given by the recurrence formula

$$n_{i+1} = n_{i-1} + 2c\Delta\delta(\delta_1 - n_i^{\alpha-1}) \ , \quad i = 2,3... \tag{2.19}$$

$$n_1 = c\delta_1^2 - c\delta_1 n_1^{\alpha-1} \tag{2.20}$$

The equilibrium condition is given by

$$\frac{q}{q_0} = 1 - n^\alpha + \alpha\delta n \tag{2.21}$$

Load-displacement relationships for various values of the spring constant c, is shown in Figure 2.4 for $\alpha = 1.5$.

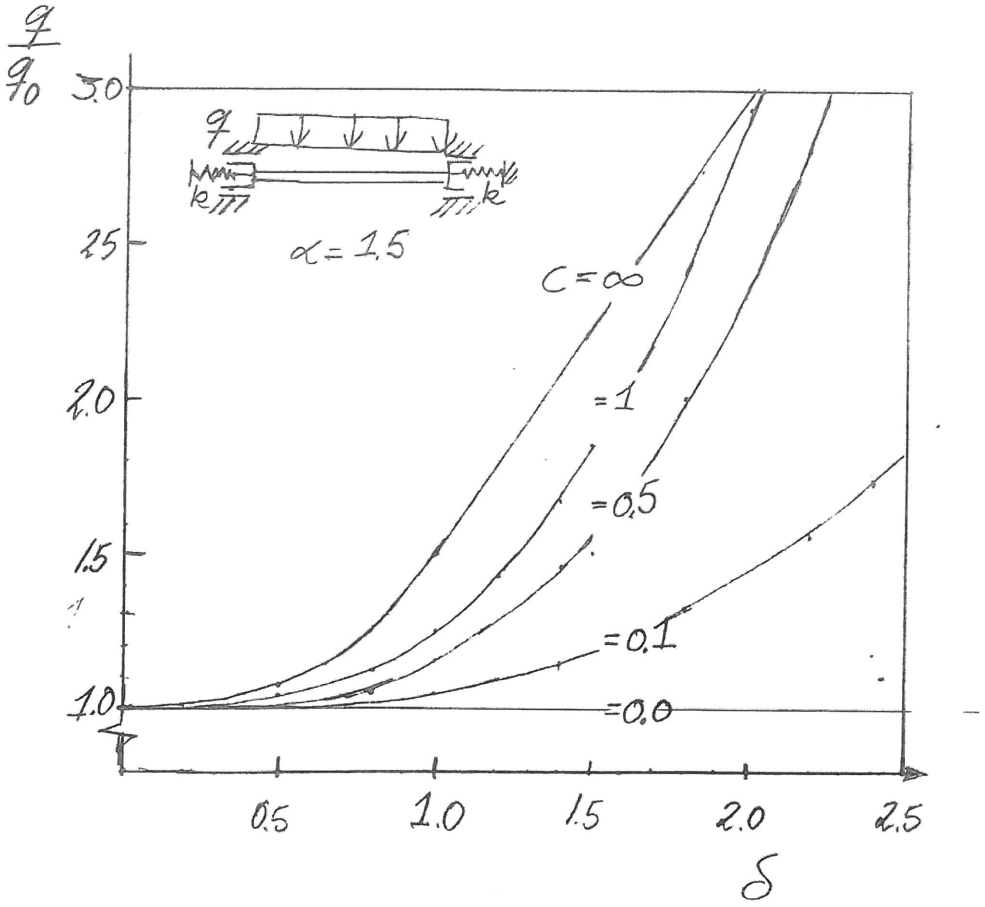

Figure 2.4 Plastic-lateral load-deformation relationships for I-profile with $\alpha = 1.5$

3. Dynamic behaviour models

Various methods are available for predicting the influence of translatory inertia on the permanent deformation of blast loaded structures. A first insight is obtained by studying the response of a linear spring mass system as shown in Fig. 5.8.

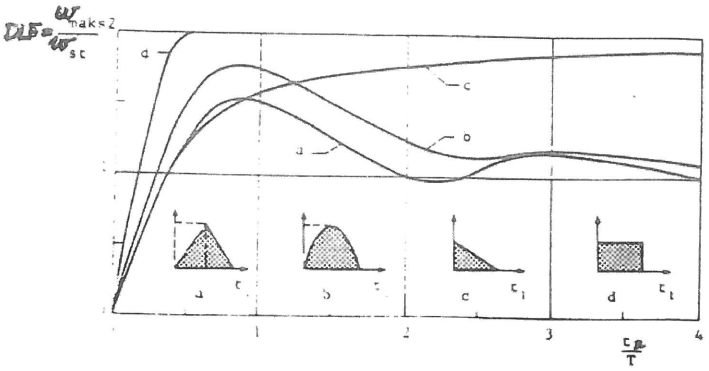

Figure 3.1 Dynamic amplification factor for four different type of loadings. T is the first natural period of vibration of the structural element /10/.

It is seen that the pulse shape, the duration as well as the rise time of the pulse is important with respect to dynamic amplification. The maximum response possible for a SDOF-system is DLA (Dynamic Load Amplification factor) = 2 for a sustained rectangular pulse.

A more realistic description of the explosion load is a skewed triangular pressure pulse. A reasonable approximation for a detonation is $t_m \approx 0.5t_p$.

As shown in Figure 3.1 the response is independent of the rise time when it is small compared to the fundamental period of vibration.

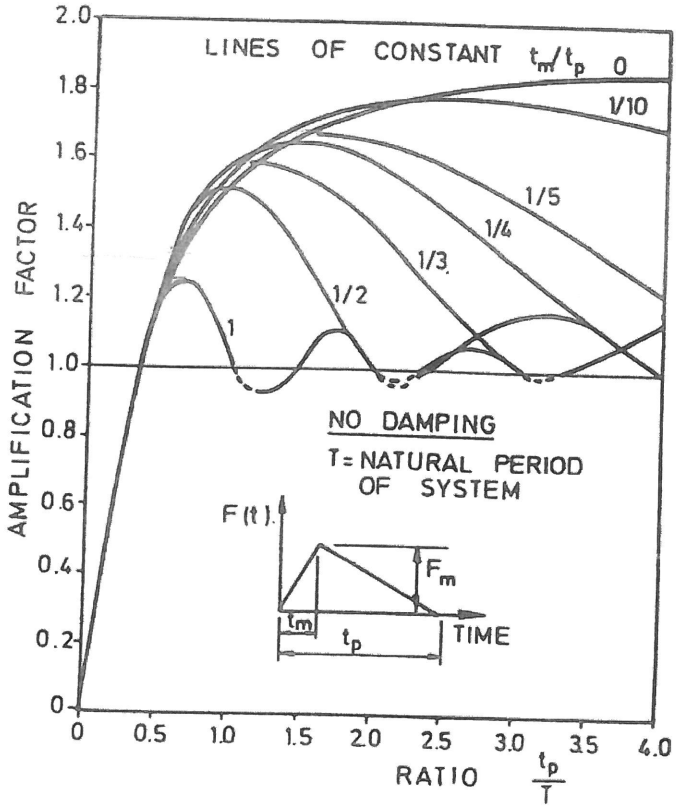

Figure 3.2 Response of a linear spring-mass system.

The results in Figure 2.4 may also be used for a beam with simply supported ends provided that the spring coefficient is taken as

$$C = \frac{N_p^3 \ell}{2k\alpha^2 M_p^2} \tag{3.1}$$

and δ is given by Equation (5.62).

A basic assumption in the consideration above is that the cross-section of the beam remains intact in the large deflection range so that the plastic bending moment is retained. This means that no twisting and lateral buckling or local buckling of webs and flanges take place.

This observation can be generalized: in the impulsive loading range, the response depends only on the total impulse and is independent of the shape of the impulse.

The results above apply to linear spring stiffness, but they are not limited to elastic material behaviour as far as maximum response in the first cycle is considered.

The rigid-plastic or elastic plastic method provide non-linear load-deformation modes can be distinguished as shown in Figure 3.3

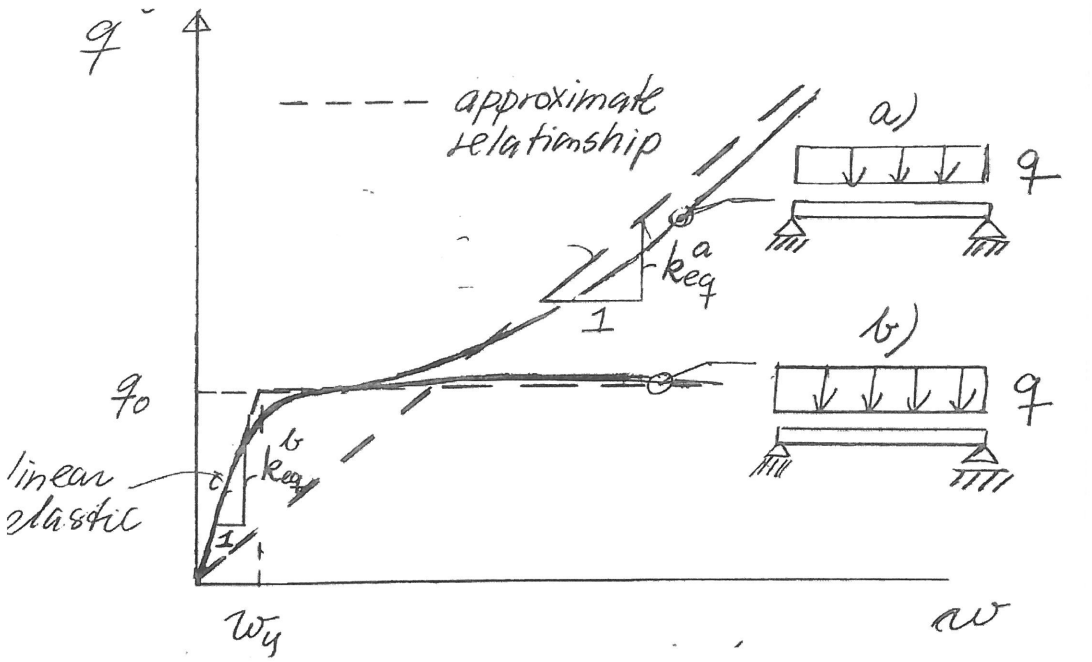

Figure 3.3 Idealized elastic-plastic response

Curve *a* describes the typical response when membrane forces are developed due to axial fixity of the ends of the beam/plate.

Curve *b* is representative for the behaviour when the axial fixity is small so that bending forces predominate the response.

A reasonable approximation for case *a* is the linear curve indicated in Figure 3.3, especially for large lateral deformation. For case *b* the bilinear representation is a valid assumption with a transition point at the deformation at the yield point, w_y, corresponding to the collapse load in bending.

Figure 3.1 may now be used to calculate the maximum response for case a deformation modes. Figure 3.4- Figure 3.7 may be used for case b deformation modes. They summarize the response of elastic plastic system.

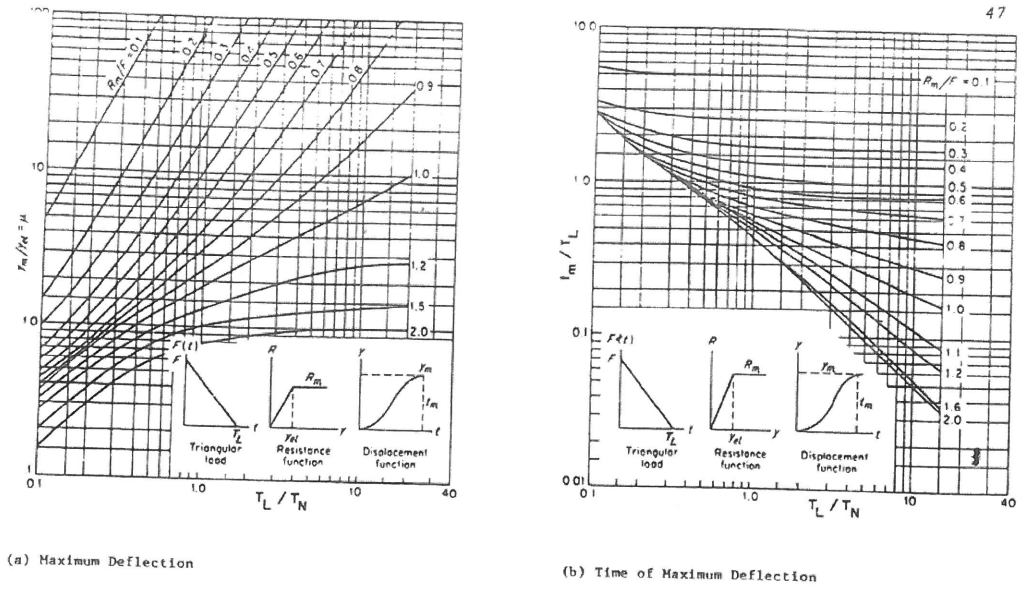

Figure 3.4 Maximum response of an Undamped One-Degree-Of-Freedom Elastic-Plastic System for a Triangular Load (U.S. Army Corps of Engineers Manual (1975)).

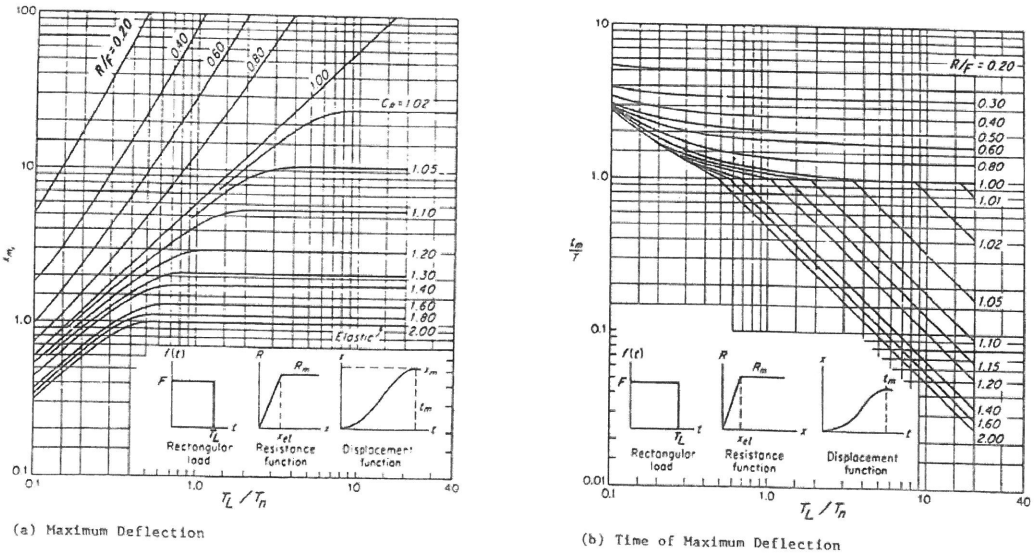

Figure 3.5 Maximum response of an Undamped One-Degree-Of-Freedom Elastic-Plastic System for a Step Load (U.S. Army Corps of Engineers Manual (1975)).

4.

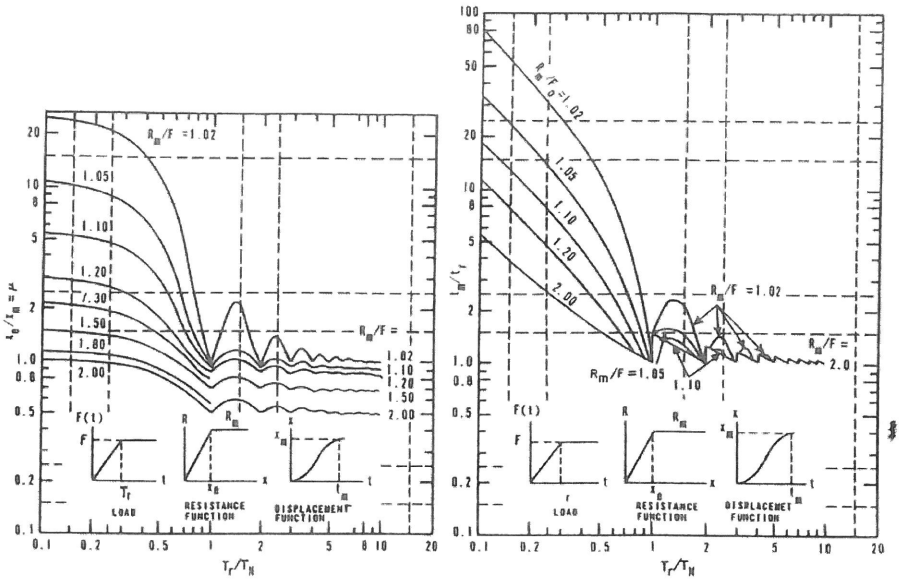

Figure 3.6 Maximum response of an Undamped One-Degree-Of-Freedom Elastic-Plastic System to Step Pulse with Finite Rise Time (U.S. Army Corps of Engineers Manual (1975)).

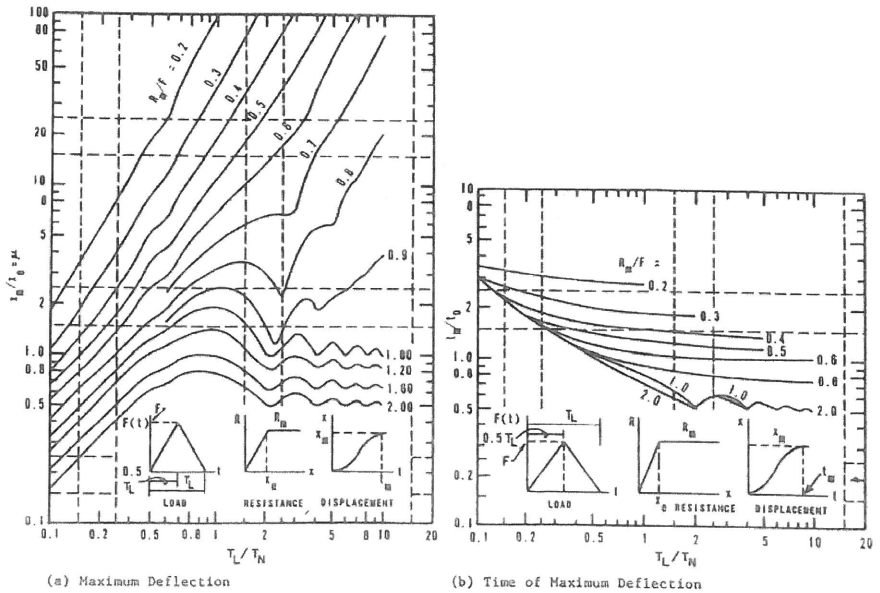

Figure 3.7 Maximum response of an Undamped One-Degree-Of-Freedom Elastic-Plastic System to Symmetrical Triangular Pulse (U.S. Army Corps of Engineers Manual (1975)).

An important factor in the above calculations is the effective natural period of vibration. This is not identical to the elastic period of vibration, but is defined according to

$$T_N = 2\pi\sqrt{\frac{m_{eq}}{k_{eq}}} \tag{3.2}$$

where k_{eq} is defined for case *a* and case *b* respectively in Figure 3.3.

The equivalent (modal) mass is calculated on the assumption that the dynamic deformation mode is identical to the static collapse pattern.

For a rectangular plate the deformation pattern shown in Figure 1.1 should be used. The equivalent plate mass should be determined so that the kinetic energy is retained, i.e.:

$$\frac{1}{2}m_{eq}v_0^2 = \frac{1}{2}\int_A \rho h v^2 dA \tag{3.3}$$

$$m_{eq} = \rho h \int_A \left(\frac{v}{v_0}\right)^2 dA \tag{3.4}$$

where v_0 is the maximum velocity at the mid hinge of the plate. ρ = mass density of plate and h = plate thickness

$$\begin{aligned} m_{eq} &= \rho h\left[\frac{1}{3}(a-b-tg\phi)b+\frac{1}{6}btg\phi\cdot b\right] \\ &= \frac{\rho h}{6}\left[2ab-b^2tg\phi\right] \end{aligned} \tag{3.5}$$

Including the minimum angle ϕ this can be written

$$m_{eq} = m_{plate}\frac{2-\alpha}{6} \tag{3.6}$$

where the total plate mass is

$$m_{plate} = \rho hab \tag{3.7}$$

Letting $b/a \to 0$ we get the relationship for a beam, i.e.

$$m_{eq} = m_{beam} \cdot \frac{1}{3} \tag{3.8}$$

For a square plate, $b/a = 1$, there is obtained

$$m_{eq} = m_{plate} \cdot \frac{1}{6} \tag{3.9}$$

3.1 Analytic solutions

Several solutions are available for rectangular plates and beams subjected to uniformly distributed pressure of constant magnitude and a certain duration (rectangular pulse).

Applying the static collapse pattern Jones (1) obtained the following formula with respect to permanent deformation at mid hinge.

$$z = \frac{3-\alpha}{2\{1+(2-\alpha)(1-\alpha)\}}\left[\left\{1+2\frac{q}{q_0}\left(\frac{q}{q_0}-1\right)(1-\cos\gamma\tau)\right\}^{1/2}-1\right] \tag{3.10}$$

where α, q/q_0 are defined in the static case, τ = duration of pulse, and

$$\gamma^2 = \frac{2q_0^*}{gh^2}\frac{\{1+(2-\alpha)(1-\alpha)\}}{(3-\alpha)} \tag{3.11}$$

ρ is mass density of plate and

$q_0^* = q_0$ for clamped plate

$q_0^* = 2q_0$ for simply supported plate

It is interesting to compare the permanent deformation predicted by Equation **(3.10)** for a long duration pulse by which $\cos\gamma\tau = -1$ with the static solution by Equation **(1.51)**.

$$z_{stat} = \frac{3-\alpha}{2(1+(2-\alpha)(1-\alpha))}\left\{\left(\frac{q}{q_0}\right)^2-1\right\}^{1/2} \tag{3.12}$$

and

$$\frac{z_{dyn}}{z_{stat}} = \frac{\left\{1+4\frac{q}{q_0}\left(\frac{q}{q_0}-1\right)\right\}^{1/2}-1}{\left\{\left(\frac{q}{q_0}\right)^2-1\right\}^{1/2}} \tag{3.13}$$

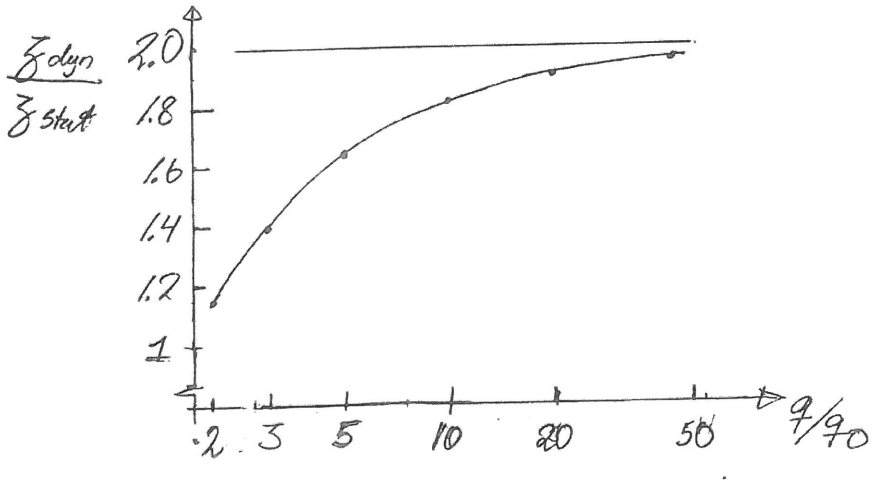

Figure 3.8 Dynamic versus static permanent deformation

It is seen from Figure 3.8 that the dynamic deformation approaches asymptotically the correct solution, $DLA = 2$ for $q/q_0 \to \infty$. The deviation may to some extent be due to the use of the approximate formula given by Equation **(1.51)**, but is mainly due to the fact that Equation **(3.10)** underestimates the permanent deformations in the small displacement range because a square yield curve is used as shown in Figure 3.9.

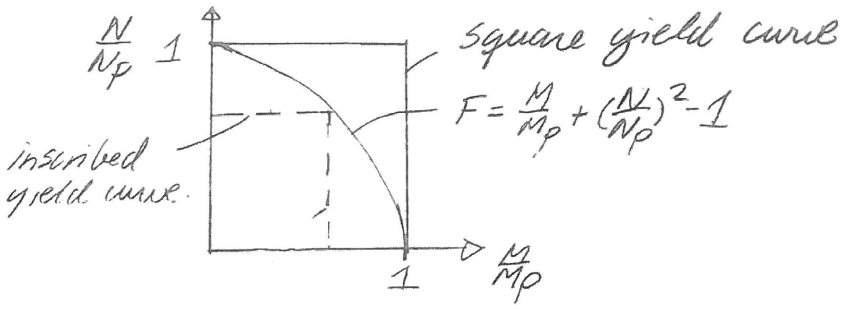

Figure 3.9 Yield curves

If an inscribed yield curve is used an upper bound to the dynamic displacement would be obtained. The corresponding curve is obtained by setting $\sigma_y = 0.618\sigma_y$. This yields

$$\frac{z_{dyn}}{z_{stat}} \in (2.58 - 3.20)$$

for

$$\frac{q}{q_0} \leftarrow (2 - 50)$$

This clearly overestimates the deformation. It is apparent from these considerations that the circumscribed square yield curve is reasonable for $z >> 1$ because the major part of the energy dissipation takes place on the membrane phase with $\frac{N}{N_p} = 1$.

The foregoing equations are also valid for beams by letting $b/a \rightarrow \infty$): $\alpha = 0$ and $b = \ell$ is beam span.

If the pressure-pulse is of short duration and $q >> q_0$ the load can be idealized as impulsive. From the moment theorem, the impulse I is given by

$$I = q\tau = \rho h V_0 \qquad (3.14)$$

where V_0 = impulsive velocity. Equation **(3.10** may be rewritten.

$$\left[1+2\frac{q}{q_0}\left(\frac{q}{q_0}-1\right)\left(1-\cos\gamma\tau\right)\right]$$
$$\approx 1+2\left(\frac{q}{q_0}\right)^2\cdot\frac{1}{2}\gamma^2\tau^2=1+\left(\frac{q}{q_0}\right)^2\gamma^2\tau^2 \qquad (3.15)$$

substituting

$$q_0=\frac{48M_p}{\alpha^2 a^2} \qquad (3.16)$$

and using Equation **(3.15)** we get

$$\Gamma=\left(\frac{q}{q_0}\right)^2\gamma^2\tau^2$$
$$=\lambda\cdot\frac{(3-2\alpha)}{6}\left\{\frac{1+(2-\alpha)(1-\alpha)}{2-\alpha}\right\} \qquad (3.17)$$

where

$$\lambda=\frac{\rho b^2 V_0^2}{4M_p} \qquad (3.18)$$

which is a non-dimensional form of the kinetic energy.

Thus, Equation **(3.10)** takes the form

$$z=\frac{(3-\alpha)}{2\left[1+(2-\alpha)(1-\alpha)\right]}\left\{1+\Gamma^{1/2}-1\right\} \qquad (3.19)$$

3.2 *A*pproximate solutions for elastic- and plastic periods of vibration

If the asymptotic solution for plastic deformation, Equation**(1.51)**, is used the plastic stiffness is given by

$$k_{eq} = \frac{d(qab)}{dw} = \frac{2q_0 ab}{h}\left\{\frac{1+(\alpha-1)(\alpha-2)}{3-\alpha}\right\} \tag{3.20}$$

the equivalent mass is given by Equation **(3.6)** and reads

$$m_{eq} = \rho abh\frac{2-\alpha}{6} \tag{3.21}$$

Hence, the "plastic" period of vibration is

$$\begin{aligned} T_{eq} &= 2\pi\sqrt{\frac{m_{eq}}{k_{eq}}} = 2\pi\sqrt{\frac{\rho h^2(3-\alpha)(2-\alpha)}{6\cdot 2q_0(1+(\alpha-1)(\alpha-2)}} \\ &= 2\pi\frac{b}{12}\sqrt{\frac{\rho}{\sigma_y}\frac{(3-2\alpha)(3-\alpha)(2-\alpha)}{(1+(\alpha-1)(\alpha-2))}} \end{aligned} \tag{3.22}$$

In the membrane phase this is valid for both clamped and rotationally free plates.

It is also seen that Eq. **(3.22)** can be written

$$\gamma = \frac{2\pi}{T_{eq}}\sqrt{\frac{3-\alpha}{6}} \tag{3.23}$$

This defines also the duration of the pulse in a more suitable way.

$$\cos\gamma\tau = \cos 2\pi\sqrt{\frac{3-\alpha}{6}}\frac{\tau}{T_{eq}} \tag{3.24}$$

Thus, $\cos\gamma\tau \approx -1$ for $\tau \geq T_{eq}$ and the maximum magnification factor is obtained.

The natural period of a clamped rectangular plate in the linear elastic range is given by

$$T_{el} = \frac{2\pi b^2}{\psi}\left\{\frac{12\rho(1-\nu^2)}{Eh^2}\right\}^{1/2} \tag{3.25}$$

where ψ = 36, 24.6, 23.2 and 22.4 when b/a = 1, ½, 1/3, and 0, respectively.

The ratio between the "plastic" and elastic period of vibration is

$$\phi = \frac{T_{eq}}{T_{el}} = \frac{\psi}{24b/h}\left\{\frac{E}{3\sigma_y(1-\nu^2)}\frac{(3-2\alpha)(3-\alpha)(2-\alpha)}{1+(1-\alpha)(2-\alpha)}\right\}^{1/2} \tag{3.26}$$

For example for $\sigma_y = 250$, $b/a = 1/3$, ϕ becomes

$\phi \approx \frac{35}{b/h}$, i.e. for $b/h > 35$

The plastic stiffness is larger than the elastic stiffness. This means that the elastic response is quite significant for high b/h-ratios.

Correspondingly, for a beam $(b/a = 0)$, $\phi \approx \frac{40}{b/h}$ i.e. almost the same ratio. For typical beams the stiffness will be governed by the plastic contribution.

3.3 Strain rate effects

For materials that are sensitive to the rate of straining the simple rigid-perfectly plastic approximations may require further refinement. For mild steel Cowper and Symonds /2/ found the following empirical relationship between the dynamic flow stress, $\sigma_y^{'}$, and the strain rate ε

$$\frac{\sigma_y^{'}}{\sigma_y} = 1 + \left(\frac{\dot{\varepsilon}}{D}\right)^{\frac{1}{p}} \tag{3.27}$$

where $D = 40$, $p = 5$ and σ_y = static (lower) yield stress. This means that the yield stress is doubled for $\varepsilon = 40s^{-1}$. The formula is well known and is often applied for dynamic correction. However, it should be noticed that it is strictly valid for the initial yield stress only. At large strains the influence of strain rate is less pronounced.

Hence, Equation **(3.27)** the formula should be used with great care when large plastic deflections are assumed. D = 4000 is proposed for such cases in Ref. /3/. Integration must be carried out over the cross-section in order to assess the influence on stress resultants. In Ref. /3/ it was proposed to use Equation **(3.21)** for beams with λ/n instead of λ where

$$n = 1 + \left[\frac{h^2 \lambda^{\frac{3}{2}}}{6D\ell^3} \left(\frac{\sigma_y}{\rho} \right)^{\frac{1}{2}} \right]^{\frac{1}{p}} \tag{3.28}$$

Alternatively, it is suggested that Equation **(3.24)** for beams and Equation. **(3.20)** for plates are used without rate correction.

3.4 Comparison with experimental data

Figure 3.10 - Figure 3.12 show comparisons between various theoretical calculations and experimental data. Curve (3) in Fig. 5.17 results from Equation. **(3.19)**with $\alpha = 0$ and $\Gamma = 3/4\lambda$.

It is seen that curve (3) overestimates the response. This is considered to be due to strain rate effect and may be accounted for by increasing the yield stress.

Curve (2) in Figure 3.11 - Figure 3.12 is identical to Equation **(3.19)** with $\alpha = 0.734$. It appears that the predictions are in much better accordance with the test results for steel and aluminum plates.

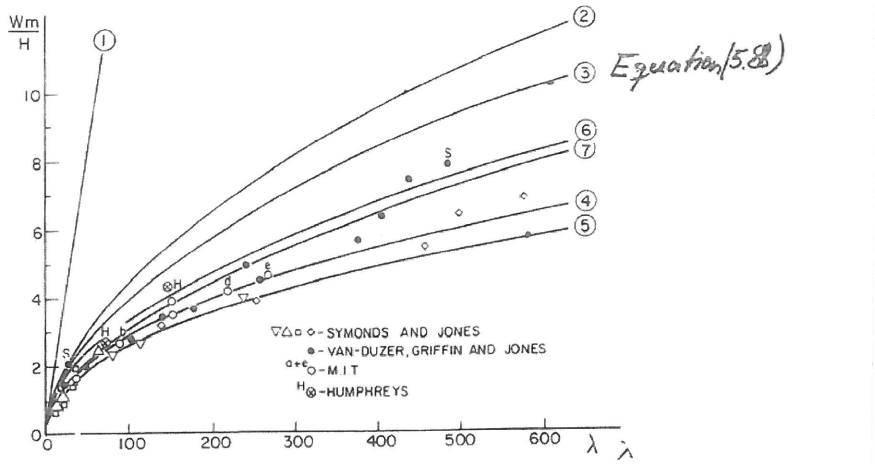

Figure 3.10 Comparison with other models and with test results on mild steel (curve 1 – bending theory, curve 2 – Symonds and Jones (19) without strain rate correction, curve 3 – Jones (7), curves 4, 5 – Symonds and Jones including strain rate effect, curve 6 – present model (hinged supports), curve 7 – present model (clamped supports)).

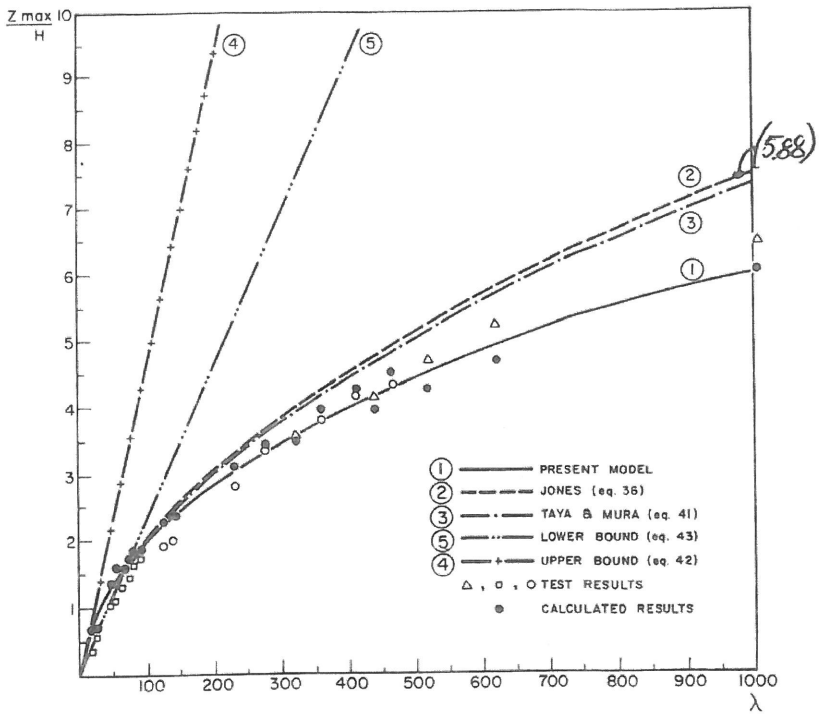

Figure 3.11 Comparison with test results – mild steel plates (curve 1 – present model, curve 2 – Jones (equation 36), curve 3 – Raya and Mura (equation 41), curve 4 – upper bound (equation 42), curve 5 – lower bound (equation 43)).

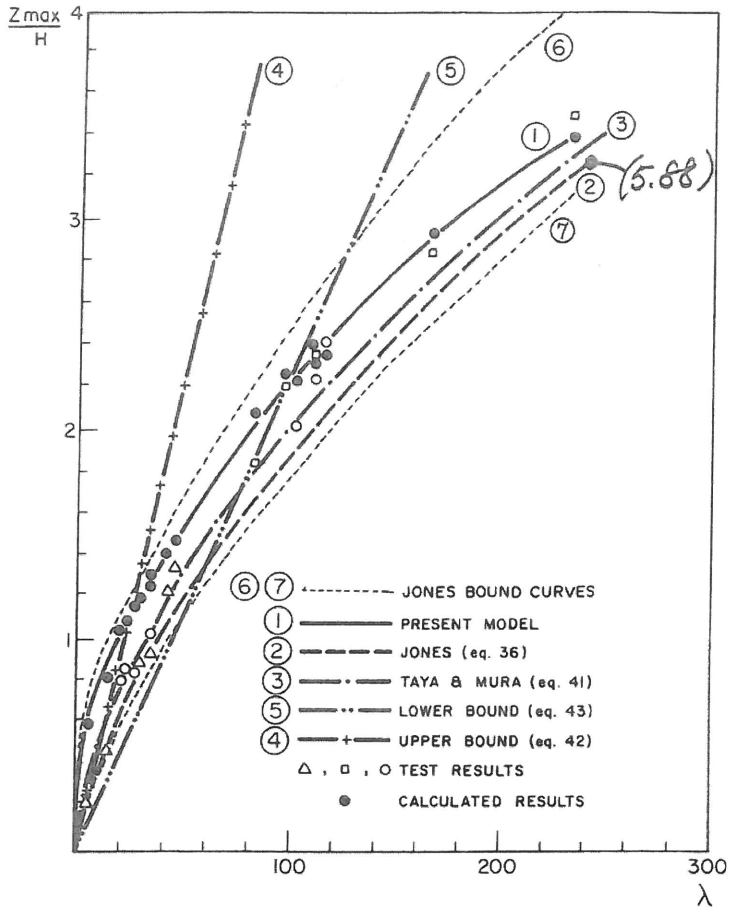

Figure 3.12 Comparison with test results. Aluminium 6016-T6 plates (curve 1 - present model, curve 2 – Jones (equation 36), curves 3 – Taya and Mura (equation 41), curve 4 – upper bound (equation 42), curve 5 – lower bound (equation 43), curves 6, 7 – Jones bound curve (41)).

References

1 Jones, N.: "A Theoretical Study on the Dynamic Plastic Behaviour of Beams and Plates with Finite Deflections". Int. Journal of Solids and Structures, Vol. 4, 1968, pp. 593-603.

2 Symonds, P.S.: "Visco-Plastic Behaviour in Response of Structures to Dynamic Loading, N.J. Huffington, ed., ASME, 1965, pp. 106-124.

3 Toni, M. and Funahashi, A.: "Energy Absorption by the Plastic Deformation of Body Structural Members", SAE Paper No. 780368, SAE, Inc., 1978.